

Article

# Synthesis and Single Crystal Growth by Floating Zone Technique of $\text{FeCr}_2\text{O}_4$ Multiferroic Spinel: Its Structure, Composition, and Magnetic Properties

 Ruslan Batulin , Mikhail Cherosov , Airat Kiiamov , Almaz Zinnatullin , Farit Vagizov, Dmitrii Tayurskii and Roman Yusupov 

Institute of Physics, Kazan Federal University, Kremlyovskaya Str., 18, Kazan 420008, Russia

\* Correspondence: tokamak@yandex.ru

**Abstract:** We present the new synthesis route of spinel-structure  $\text{FeCr}_2\text{O}_4$  and its single crystal growth by the optical floating zone method, ensuring its single phase and near-ideal composition. The advantage of the proposed synthesis method is the creation of the reducing atmosphere in the oven needed for preserving the  $\text{Fe}^{2+}$  oxidation state via decomposition of the iron (II) oxalate  $\text{FeC}_2\text{O}_4$  used as one of the initial components. The occurrence of the  $\text{Fe}^{3+}$  ions in the obtained polycrystalline samples as well as grown single crystals was carefully monitored by means of Mössbauer spectroscopy. Magnetic susceptibility and heat capacity temperature dependences reveal a sequence of the structural (138 K) and magnetic (at 65 K and 38 K) phase transition characteristics for the  $\text{FeCr}_2\text{O}_4$  compound.

**Keywords:** multiferroic spinel; floating zone; single crystal; Mössbauer spectroscopy



**Citation:** Batulin, R.; Cherosov, M.; Kiiamov, A.; Zinnatullin, A.; Vagizov, F.; Tayurskii, D.; Yusupov, R. Synthesis and Single Crystal Growth by Floating Zone Technique of  $\text{FeCr}_2\text{O}_4$  Multiferroic Spinel: Its Structure, Composition, and Magnetic Properties. *Magnetochemistry* **2022**, *8*, 86. <https://doi.org/10.3390/magnetochemistry8080086>

Academic Editors: Kamil Gareev and Ksenia Chichay

Received: 30 June 2022

Accepted: 31 July 2022

Published: 5 August 2022

**Publisher's Note:** MDPI stays neutral with regard to jurisdictional claims in published maps and institutional affiliations.



**Copyright:** © 2022 by the authors. Licensee MDPI, Basel, Switzerland. This article is an open access article distributed under the terms and conditions of the Creative Commons Attribution (CC BY) license (<https://creativecommons.org/licenses/by/4.0/>).

## 1. Introduction

Crystalline materials with the spinel structure and a general chemical formula of  $\text{MM}_2\text{X}_4$  have been studied for several decades due to a broad range of magnetic, structural, and dielectric properties discovered in them [1–7]. Here, M and M' are metal ions or a combination of them, and X represents oxygen or some chalcogen divalent anion ( $\text{S}^{2-}$ ,  $\text{Se}^{2-}$ ,  $\text{Te}^{2-}$ ). Among them, the iron chromite  $\text{FeCr}_2\text{O}_4$  spinel is a well-known compound with a normal cubic spinel structure at room temperature (space group  $Fd\bar{3}m$ , Figure 1) and the lattice constant  $a = 8.378 \text{ \AA}$  [8]. The tetrahedrally coordinated A-site in it is occupied by  $\text{Fe}^{2+}$  ions (electronic configuration  $3d^6$ ) and the octahedrally coordinated B site is occupied by  $\text{Cr}^{3+}$  ions (electronic configuration  $3d^3$ ).

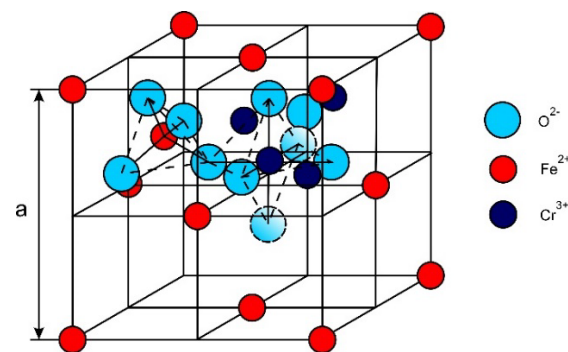


**Figure 1.** Unit cell of the  $\text{FeCr}_2\text{O}_4$  compound with a spinel structure. Ions in the quarter of the unit cell are shown.

Another cation distribution exists in the inverse spinel: one-half of the trivalent cations fill the A-positions and another half is randomly distributed over the B-site network

together with the divalent ions. Recently, inverse spinels also attracted the attention due to their peculiar magnetic and electronic properties [9,10].

In  $\text{FeCr}_2\text{O}_4$ , on cooling below  $\sim 140$  K, symmetry lowering of the crystal structure occurs due to the cooperative Jahn–Teller effect within the A-ion sublattice. The electronic ground state of the  $\text{Fe}^{2+}$  ions in high-symmetry tetrahedral oxygen coordination is the  ${}^5\text{E}$  orbital doublet that is strongly coupled to the E-symmetry distortions. The ground state of the  $\text{Cr}^{3+}$  ion in octahedral surrounding is the orbital singlet  $\text{A}_{2g}$ , which is not the Jahn–Teller active. The strong interaction between the degenerate states and the local lattice distortions leads to an effective strong coupling between the adjacent ( $\text{FeO}_4$ ) structural units. Below a critical temperature  $T_{\text{OO}}$ , a structural phase transition from the cubic to tetragonal symmetry occurs due to the orbital ordering. For  $\text{FeCr}_2\text{O}_4$ , the critical temperature is  $T_{\text{OO}} = 135$  K, and the tetragonal distortion achieves a value of  $c/a = 0.986$  [11,12]. It was shown also that the cubic-to-tetragonal transition temperature  $T_{\text{OO}}$  gradually decreases if the Jahn–Teller-active  $\text{Fe}^{2+}$  ions are replaced by the “inactive” high-spin  $\text{Mn}^{2+}$  ions (electronic configuration  $3d^5$ , ground state is the  $\text{A}_{1g}$  orbital singlet), related to the weakening of the effective long-range orbital–orbital interaction [13]. On further cooling, the symmetry of the  $\text{FeCr}_2\text{O}_4$  crystal structure is lowered to orthorhombic, almost simultaneously with an establishment of the magnetic order at  $\sim 70$  K [13].

The magnetic properties of the oxide spinel  $\text{FeCr}_2\text{O}_4$  are more complex than, for example, of its sulphide representative  $\text{FeCr}_2\text{S}_4$ ; the latter can be described by the Neel model and exhibits a transition to collinear ferrimagnetic state at  $T_{\text{N}} = 180$  K [8]. A powder neutron diffraction study has shown that the spin arrangement in  $\text{FeCr}_2\text{O}_4$  is collinear ferrimagnetic between  $T_{\text{N}} = 80$  K and  $T_{\text{S}} = 35$  K. It is important to mention that the transition temperature  $T_{\text{N}}$  strongly depends on the amount of the  $\text{Fe}^{3+}$  ions formed during the synthesis procedure [14]. Below 35 K, according to [8], a cone spiral spin structure is established in  $\text{FeCr}_2\text{O}_4$ . Such a ferrimagnetic spiral structure has been established in cubic spinel  $\text{MnCr}_2\text{O}_4$  also [15], and the model for tetragonal spinel was developed earlier by Menyuk et al. [16]. However, the proposed spiral spin structure is currently under a debate, and high-quality single-crystal samples of  $\text{FeCr}_2\text{O}_4$  are needed for its appropriate examination by either the neutron diffraction or, e.g., the Mössbauer effect studies [17–19]. Recently, the magnetic and structural properties of the  $\text{Fe}_{1+x}\text{Cr}_{2-x}\text{O}_4$  ( $0 \leq x \leq 1$ ) spinel series have been investigated [14]. It has been found that partial replacement of  $\text{Cr}^{3+}$  ions by  $\text{Fe}^{3+}$  ones leads to an increase in the paramagnetic to collinear ferrimagnetic transition temperature  $T_{\text{N}}$  but reduces the collinear to spiral spin structure temperature  $T_{\text{S}}$ .

Lately, the interest to the 3d-metal spinel family renewed due to a discovery of magnetoelectric effects and related to it multiferroicity [20]. Mutual dependence of the magnetic and dielectric properties gives rise to such practically important phenomena as nonreciprocity [21] or magnetic field-controlled optical diodes [22,23]. Thus, spinels are intensely investigated and attract an attention of the researchers both from the fundamental science and its applied field.

Iron chromite  $\text{FeCr}_2\text{O}_4$  is a compound for which many aspects remain uncovered, such as an intrinsic magnetic structure and its development with temperature and an applied magnetic field, an origin of the induced electric polarization and magnetoelectric coupling. The main source of the observed discrepancies and debates, probably, is the quality and stoichiometry of the studied samples. Indeed, whatever the synthesis route is used, almost inevitably, part of the  $\text{Fe}^{2+}$  ions oxidize to the  $\text{Fe}^{3+}$  state and then compete with  $\text{Cr}^{3+}$  ions for the octahedral B-sites [24]. A fact of such substitution cannot be resolved by the easily accessible X-ray diffractometry (XRD), but, as it was mentioned above, can affect a material's properties notably. To preserve the desired  $\text{Fe}^{2+}$  state, a reducing atmosphere is created traditionally in an oven during the solid-state synthesis by admixing of either the hydrogen  $\text{H}_2$  or carbon monoxide  $\text{CO}$  to an inert gas (argon, nitrogen, or  $\text{CO}_2$ ) [25]. This complicates the procedure but does not ensure an absence of  $\text{Fe}^{3+}$  ions in the product. We propose a synthesis approach that does not require an involvement of additional reducing agents though produces a minimal amount of  $\text{Fe}^{3+}$  ions at the output of the solid-state

synthesis. The single crystal samples were grown by the floating zone method, and we find that in the crystal an amount of  $\text{Fe}^{3+}$  ions is left the same as in a prepared ceramic ingot. Basic properties of the grown single-crystal sample are described. A preliminary study of the sample has revealed the magnetic structure rearrangement under an applied magnetic field at  $\sim 21$  K accompanied by an appearance of the butterfly-like magnetic hysteresis [21].

The article is written as follows: in Section 2 the sample preparation procedure is described as well as the characterization methods used, Section 3 presents the results of the XRD analysis and Mössbauer spectroscopy of the as-grown and annealed single crystal of  $\text{FeCr}_2\text{O}_4$ , in Section 4 the magnetic susceptibility is presented together with a specific heat data, and in the Conclusions the obtained structural and magnetic transition temperatures are summarized and compared with results obtained earlier.

## 2. Sample Preparation and Experimental Methods

The polycrystalline  $\text{FeCr}_2\text{O}_4$  sample was synthesized by solid-state reaction using the iron (II) oxalate dihydrate  $\text{FeC}_2\text{O}_4 \times 2\text{H}_2\text{O}$  (Alfa Aesar, 99.999%) and chromium (III) oxide  $\text{Cr}_2\text{O}_3$  (Alfa Aesar, 99.995%) as starting reagents. The reagents were mixed in a stoichiometric ratio, and the actual weight of iron (II) oxalate was adjusted based on the measured thermogravimetric analysis (TGA) results. The stoichiometric mixture was thoroughly ground and mixed in the air for 3 h in an agate mortar. The mixture in an alumina crucible was placed to the vertical furnace (MTI GSL1700X). The chamber was evacuated to  $10^{-2}$  mbar and purged with the pure Ar (99.9998%) several times. The synthesis took place in a weak flow of argon ( $\sim 0.01$  L/min) under slight over pressure ( $\sim 0.01$  bar) at a temperature of  $1400$  °C for 12 h. According to TGA, on heating, iron (II) oxalate dehydrate first releases water (by achieving  $\sim 175$  °C) and then, in the range of  $200$ – $300$  °C, decomposes following a reaction of



Carbon monoxide emitted during the decomposition inhibits the oxidation of FeO, thus preserving the  $\text{Fe}^{2+}$  state of the iron ions. The resulting reaction product was examined for the formation of the desired phase by the powder XRD analysis and for a presence of the undesired  $\text{Fe}^{3+}$  ions by the Mössbauer spectroscopy. The powder was thoroughly grounded, mixed with the GE varnish in a 19:1 volume ratio with the addition of the extra pure isopropyl alcohol, pressed into a cylindrical rod and fired at a temperature of  $1400$  °C for 2 h in a weak flow of pure argon.

A single crystal of  $\text{FeCr}_2\text{O}_4$  was grown in a pure argon flow of  $0.1$  L/min at a pressure of  $5.5$  bar by the floating zone method with optical heating using the FZ-T-4000-H-VII-VPO-PC furnace (Crystal Systems Corp., Yamanashi, Japan) equipped with four 1-kW halogen lamps (Crystal Systems Corp., Yamanashi, Japan). A relatively high growth rate of  $5$ – $8$  mm/hour was used. The feed and seed rods were counter rotated at the rates of  $10$  and  $15$  rpm, respectively, to obtain a homogeneous molten zone. The as-grown crystal (Figure 2) was afterwards annealed for  $154$  h at a temperature of  $1200$  °C in argon. Both the as-grown sample and the one after calcination were examined with the powder XRD and the Mössbauer spectroscopy.



**Figure 2.** A picture of the  $\text{FeCr}_2\text{O}_4$  crystal grown by the optical floating zone method (see text).

XRD measurements were carried out with the Bruker D8 Advance diffractometer (Bruker AXS GmbH, Karlsruhe, Germany) equipped with the  $\text{Cu-K}\alpha$  source (Siemens AG,

Berlin, Germany) at room temperature (RT). For the measurements, samples were carefully ground in an agate mortar to a fine powder state. The single-crystal structure of the grown sample was verified by means of the two-dimensional  $\chi$ - $\varphi$  scan of the sample mounted to the Euler cradle with the  $2\theta$ -angle adjusted to a definite XRD-maximum.

Mössbauer effect studies in the transmission geometry were carried out with the conventional spectrometer (WissEl GmbH, Starnberg, Germany), operating in a constant acceleration mode, at RT.  $^{57}\text{Co}$  (Rh) (RITVERC JSC, St. Petersburg, Russia) with the activity of about 40 mCi was used as source of the resonance radiation. The spectrometer velocity scale was calibrated using spectrum of thin metallic iron foil at RT. The spectra were fitted using the SpectrRelax (v. 2.1, Matsnev, M.E.; Rusakov, V.S.; Moscow, Russia) software [26]. Values of the isomer shift are reported versus the center of gravity of the  $\alpha$ -Fe at RT. For the measurements, finely ground powders were used for preparing thin Mössbauer absorbers.

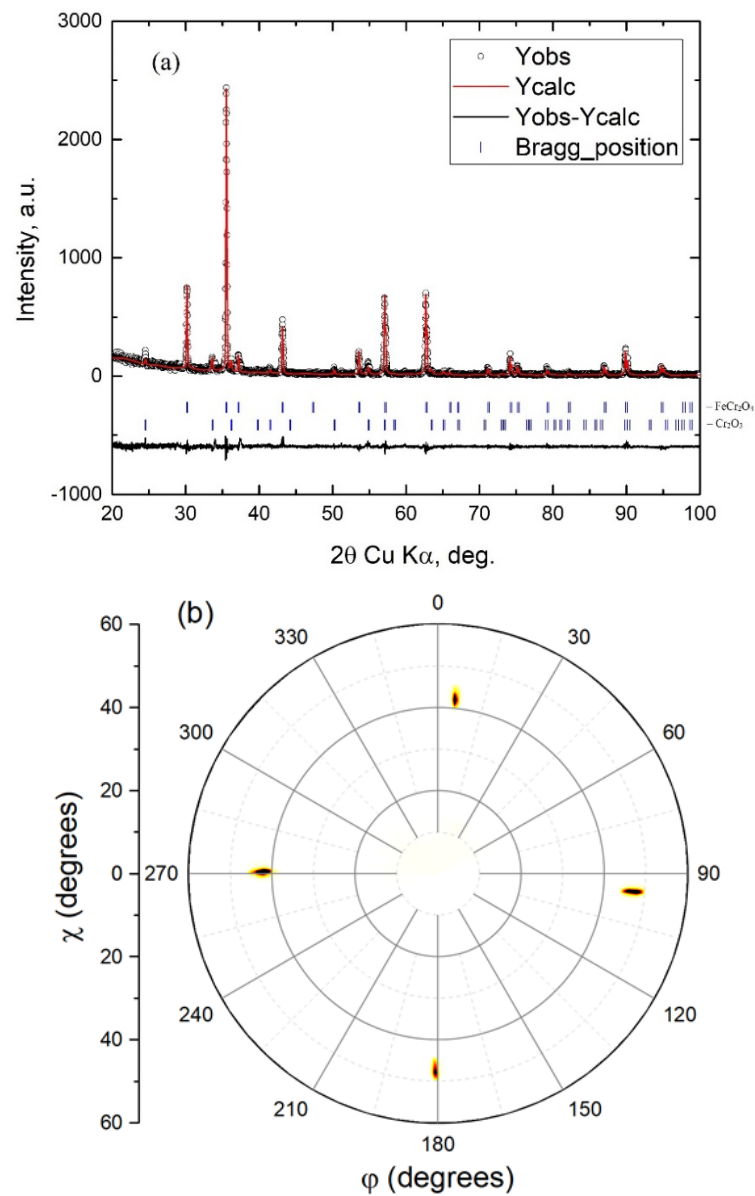
Magnetization of the single crystal of the  $\text{FeCr}_2\text{O}_4$  as a function of the magnetic field and temperature was measured using the Physical Property Measurement System (PPMS-9) by Quantum Design with a vibrating sample magnetometry (VSM) option. Heat capacity measurements in zero applied magnetic field at temperatures from 5 to 300 K were also carried out with the PPMS-9 with a heat capacity option using a  $2\tau$  relaxation approach.

### 3. XRD and Mössbauer Spectroscopy

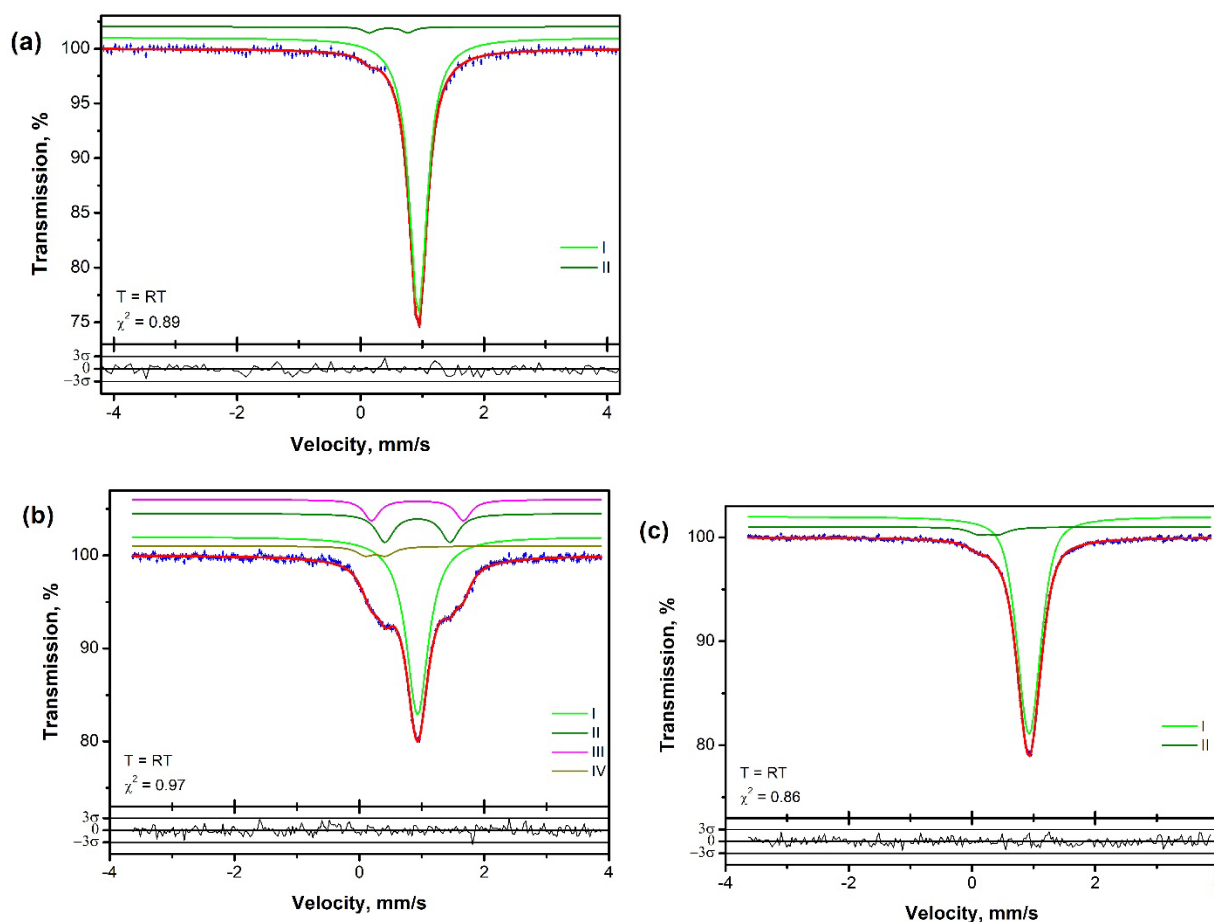
The powder XRD pattern of the crashed single crystal of  $\text{FeCr}_2\text{O}_4$  and its Rietveld-refined model curve are shown in Figure 3a. The calculated model has revealed a dominating spinel structure—an  $\text{FeCr}_2\text{O}_4$  (94%) phase and an impurity  $\text{Cr}_2\text{O}_3$  (6%) phase. Lattice parameter  $a$  of the spinel phase was equal to 8.375 Å, which is in a good agreement with data published in the literature [8,27]. Two reasons can be proposed to explain an occurrence of the residual  $\text{Cr}_2\text{O}_3$  phase: (i) partial transformation of the  $\text{Fe}^{2+}$  ions to the  $\text{Fe}^{3+}$  state (see below) and (ii) a slight departure from the initial mixture stoichiometry due to unsaturated in-water iron (II) oxalate dihydrate.

Figure 3b presents the result of the  $\chi$ - $\varphi$  scan of the grown sample of the  $4 \times 4 \times 2 \text{ mm}^3$  size with the near (001)-oriented large faces and  $2\theta$ -angle = 62.72 degrees corresponding to the {440}-type reflections. Observation of the expected four diffraction maxima within the scanned solid angle and an absence of any additional detected signals for this arrangement undoubtedly indicates the single-crystal structure of the grown macroscopic sample.

The RT Mössbauer spectrum of the polycrystalline  $\text{FeCr}_2\text{O}_4$  used after for the single-crystal growth is shown in Figure 4a. The spectrum may be reasonably well fitted with a sum of two components; namely, the major singlet with the relative area of  $A = 97(1)\%$  and the minor doublet with  $A = 3(1)\%$ . The isomer shift of the singlet  $\delta = 0.94(1) \text{ mm/s}$  is the characteristic for the high-spin  $\text{Fe}^{2+}$  ions in the tetrahedral oxygen coordination (A-site in the spinel structure) and matched well the reported earlier results [19]. The lineshape of the singlet is the Lorentzian with the width value of  $w = 0.34(1) \text{ mm/s}$ . The latter value is slightly larger than the one expected for iron-bearing crystalline powders ( $w \sim 0.3 \text{ mm/s}$ ) and may be explained by the broadening due to a dynamic tetragonal distortion reorientation related to the dynamic Jahn–Teller effect [19]. The doublet with the isomer shift of  $\delta = 0.46(3) \text{ mm/s}$  and the quadrupole splitting  $2\epsilon = 0.63(6) \text{ mm/s}$  may be associated with the high-spin  $\text{Fe}^{3+}$  ions in the octahedral oxygen coordination, i.e., in the B-sites of the spinel structure.



**Figure 3.** Powder XRD pattern of ground single crystal and its Rietveld refined model curve (a) and the 2D  $\chi$ - $\phi$  scan of the  $\text{FeCr}_2\text{O}_4$  single crystal with  $2\theta$ -angle = 62.72 degrees corresponding to the {440} X-ray diffraction maximum (b).



**Figure 4.** Mössbauer spectra at room temperature of (a) polycrystalline  $\text{FeCr}_2\text{O}_4$  powder used for the crystal growth, (b) as grown single crystal  $\text{FeCr}_2\text{O}_4$ , and (c) after the post-annealing (see text).

The RT Mössbauer spectra of the as-grown and the post-annealed crystals are depicted in Figure 4b,c, respectively. The spectrum of the as-grown crystal was fitted with a sum of four components; namely, one singlet and three doublets. The singlet with  $\delta = 0.93(1)$  mm/s,  $w = 0.43(1)$  mm/s, and  $A = 67(1)\%$  matches with the analogous signal in the spectrum of the polycrystalline  $\text{FeCr}_2\text{O}_4$ . An additional broadening of this component may be related to the microstresses in the crystal. The isomer shift values of the two doublets are the same as that of the singlet (the values were fixed during the fitting), whereas the quadrupole splitting values are  $1.04(3)$  mm/s and  $1.47(3)$  mm/s and the relative areas  $17(4)\%$  and  $11(3)\%$ , respectively. It shows that these  $\text{Fe}^{2+}$  ions have the electronic configurations close to the one if the ions are manifested by the singlet, but some electric field gradients (EFG) are present in these centers. We suppose that these EFGs are associated with residual static bulk distortions revealed in the XRD patterns of the as-grown sample by the complex shapes of the diffraction maxima. As the result of the annealing, these doublets totally vanished, which proved our claim. After the annealing, the singlet parameters were  $\delta = 0.93(1)$  mm/s and  $A = 95(1)\%$ . However, its lineshape deviated from the Lorentzian and the spectrum was fitted assuming its pseudo-Voigt profile. The Lorentzian width for the singlet was estimated as  $w = 0.46(1)$  mm/s, and the parameter  $\alpha$  value defined in Ref. [28] was  $0.47(2)$ . The deviation of the lineshape from the Lorentzian, most probably, is related to some distribution of the hyperfine parameters. The residual microstresses may introduce local EFGs with some distribution. These microstresses were also visible from the XRD reflexes broadening.

The hyperfine parameters of the minor doublet in the spectra of as-grown and post-annealed samples are  $\delta = 0.26(2)$  mm/s,  $2\epsilon = 0.32(3)$  mm/s,  $A = 5(1)\%$  and  $\delta = 0.27(2)$  mm/s,  $2\epsilon = 0.32(3)$  mm/s,  $A = 6(1)\%$ , respectively. The isomer shift and quadrupole splitting

values of the minor doublet after growth and annealing notably differ from the values of the minor doublet in the spectrum of the polycrystalline  $\text{FeCr}_2\text{O}_4$ ; they are more characteristic for the high-spin  $\text{Fe}^{3+}$  ions in the tetrahedral oxygen coordination, i.e., in the A-site of the spinel structure. The presence of the  $\text{Fe}^{3+}$  ions in the A-sites indicates a partial inversion of the nominally normal spinel structure of  $\text{FeCr}_2\text{O}_4$ . The same quantity of divalent ions should occupy the B sites. However, such a component is not resolved in our spectra.

#### 4. Specific Heat and Magnetic Susceptibility Results

Both the specific heat and magnetic susceptibility were studied on the post-annealed single crystal  $\text{FeCr}_2\text{O}_4$  sample.

The specific heat  $C_p$  was measured in the temperature range of 5–300 K (Figure 5). It reveals a sequence of the anomalies observed on cooling below 200 K. The first phase transition corresponding to an establishment of the long-range orbital ordering within the A-sites takes place at the temperature of  $T_{\text{OO}} = 138$  K, which is within an experimental uncertainty the same as reported by Kose et al. [29]. On further cooling, the next anomaly is found at  $\sim 65$  K, close to the reported Neel temperature accompanied by the structural transition from the tetragonal to the orthorhombic phase. We note here that the obtained value of the Neel temperature is probably the lowest reported in the literature and recalling its increase with the concentration of  $\text{Fe}^{3+}$  ions, we can assume that the obtained single crystal is characterized by the chemical composition most close to an ideal [14]. At  $T_s = 38.5$  K, another anomaly in  $C_p(T)$  dependence is found, which, according to the neutron diffraction data [8], corresponds to a development of a non-collinear conical spin state. This value is slightly higher than the value of 38 K obtained by Singh et al. from dielectric permittivity measurements [20].

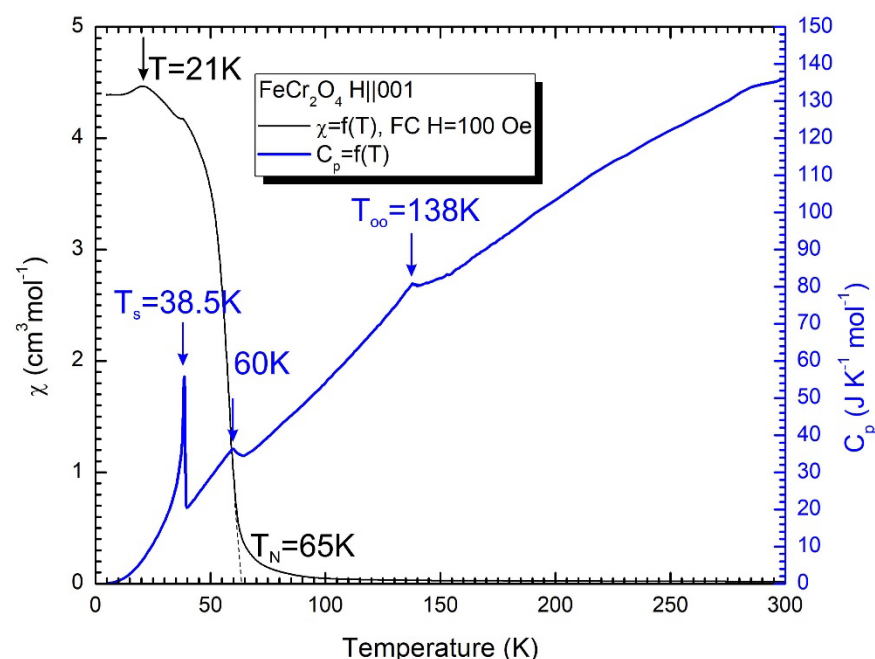


**Figure 5.** The temperature dependence of magnetic susceptibility and specific heat for  $\text{FeCr}_2\text{O}_4$ . Black line is the result of the field-cooled (FC) at  $H = 100$  Oe measurements, respectively, the blue line represents the specific heat data.

Magnetic susceptibility was measured with the magnetic field applied along the quasi-cubic [001] direction. The temperature dependence of the magnetic susceptibility of the  $\text{FeCr}_2\text{O}_4$  in the field of  $H = 100$  Oe is shown in Figure 5. An onset of the collinear ferrimagnetic state is clearly revealed at  $\sim 65$  K, matching an anomaly in the specific heat data. Another weak, though clearly resolved, anomaly is found at  $\sim 38$  K again matching a peak in  $C_p(T)$ , and, at  $\sim 21$  K, the susceptibility drops. This anomaly is not reflected

in the specific heat data. In our recent paper [21], we have found that the shape of the magnetic susceptibility dependence of the grown  $\text{FeCr}_2\text{O}_4$  single-crystal on temperature is strongly modified with the variation of an applied magnetic field; moreover, the shape of the magnetic hysteresis loop changes from a conventional to the butterfly-like one. We have tentatively assigned this observation to the spin structure rearrangement similar to that reported for the isostructural  $\text{FeCr}_2\text{S}_4$  compound [30]. The authors also observed the butterfly-like hysteresis loop and assigned it to an unconventional magnetic-field-induced spin-reorientation transition for the single crystal  $\text{FeCr}_2\text{S}_4$  with an orbitally ordered ground state of  $\text{Fe}^{2+}$  [30]. Similar butterfly-like hysteresis loops were observed for other systems (for example, LCMO manganite with  $T_N \approx 50$  K) [31].

## 5. Conclusions

In this article, we report on the successful synthesis of both the powder by the high-temperature solid-state reaction and the single crystal  $\text{FeCr}_2\text{O}_4$  using iron (II) oxalate and chromium (III) oxide as starting materials. The crystal structure and phase composition were approved by the powder X-ray diffraction method. The presence of  $\text{Fe}^{3+}$  ions in the grown crystal was analyzed by Mössbauer spectroscopy. The heat capacity measurements show three peaks corresponding to structural and magnetic phase transitions at 138 K, 65 K, and 38.5 K. The observed value of the Neel temperature  $T_N = 65$  K to our knowledge is the lowest reported in literature, indicating the lowest amount of  $\text{Fe}^{3+}$  ions in the synthesized sample.

**Author Contributions:** Conceptualization, R.B. and R.Y.; methodology, A.Z., A.K., M.C.; formal analysis, A.Z., A.K. and M.C.; investigation, M.C, A.Z. and A.K.; resources, D.T. and R.Y.; writing—original draft preparation, R.B. and R.Y.; writing—review and editing, R.Y., R.B., M.C. and A.Z.; visualization, R.B. and A.Z.; supervision, R.Y., D.T. and F.V. All authors have read and agreed to the published version of the manuscript.

**Funding:** The reported studies were performed with the support from the Russian Science Foundation, project No. 19-12-00244.

**Data Availability Statement:** The data presented in this study are available on request from the corresponding author. The data are not publicly available due to privacy restrictions.

**Conflicts of Interest:** The authors declare no conflict of interest. The funders had no role in the design of the study; in the collection, analyses, or interpretation of data; in the writing of the manuscript; or in the decision to publish the results.

## References

1. Tsurkan, V.; Krug Von Nidda, H.A.K.; Deisenhofer, J.; Lunkenheimer, P.; Loidl, A. On the complexity of spinels: Magnetic, electronic, and polar ground states. *Phys. Rep.* **2021**, *926*, 1–86. [[CrossRef](#)]
2. Sundaresan, A.; Ter-Oganessian, N.V. Magnetoelectric and multiferroic properties of spinels. *J. Appl. Phys.* **2021**, *129*, 060901. [[CrossRef](#)]
3. Krupicka, S.; Novak, P. Oxide spinels. In *Handbook of Ferromagnetic Materials*; Wohlfarth, E.P., Ed.; North-Holland Publishing Company: Amsterdam, The Netherlands, 1982; Volume 3, pp. 189–304. ISBN 978-0-444-86378-2.
4. Hemberger, J.; Lunkenheimer, P.; Fichtl, R.; Krug von Nidda, H.-A.; Tsurkan, V.; Loidl, A. Relaxor ferroelectricity and colossal magnetocapacitive coupling in ferromagnetic  $\text{CdCr}_2\text{S}_4$ . *Nature* **2005**, *434*, 364–367. [[CrossRef](#)]
5. Lee, S.-H.; Broholm, C.; Ratcliff, W.; Gasparovic, G.; Huang, Q.; Kim, T.H.; Cheong, S.-W. Emergent excitations in a geometrically frustrated magnet. *Nature* **2002**, *418*, 856–858. [[CrossRef](#)] [[PubMed](#)]
6. Fritsch, V.; Hemberger, J.; Büttgen, N.; Scheidt, E.-W.; Krug von Nidda, H.-A.; Loidl, A.; Tsurkan, V. Spin and Orbital Frustration in  $\text{MnSc}_2\text{S}_4$  and  $\text{FeSc}_2\text{S}_4$ . *Phys. Rev. Lett.* **2004**, *92*, 116401. [[CrossRef](#)] [[PubMed](#)]
7. Fichtl, R.; Tsurkan, V.; Lunkenheimer, P.; Hemberger, J.; Fritsch, V.; Krug von Nidda, H.-A.; Scheidt, E.-W.; Loidl, A. Orbital Freezing and Orbital Glass State in  $\text{FeCr}_2\text{S}_4$ . *Phys. Rev. Lett.* **2005**, *94*, 027601. [[CrossRef](#)] [[PubMed](#)]
8. Shirane, G.; Cox, D.E.; Pickart, S.J. Magnetic Structures in  $\text{FeCr}_2\text{S}_4$  and  $\text{FeCr}_2\text{O}_4$ . *J. Appl. Phys.* **1964**, *35*, 954–955. [[CrossRef](#)]
9. Benhalima, C.; Amari, S.; Beldi, L.; Bouhafs, B. First-Principles Study of Ferromagnetism in Iron Chromite Spinel:  $\text{FeCr}_2\text{O}_4$  and  $\text{CrFe}_2\text{O}_4$ . *SPIN* **2019**, *9*, 1950014. [[CrossRef](#)]
10. Santos-Carballal, D.; Roldan, A.; Grau-Crespo, R.; de Leeuw, N.H. First-principles study of the inversion thermodynamics and electronic structure of  $\text{FeM}_2\text{X}_4$  (thio)spinels ( $M=\text{Cr, Mn, Co, Ni}$ ;  $X=\text{O, S}$ ). *Phys. Rev. B* **2015**, *91*, 195106. [[CrossRef](#)]

11. Whipple, E.; Wold, A. Preparation of stoichiometric chromites. *J. Inorg. Nucl. Chem.* **1962**, *24*, 23–27. [[CrossRef](#)]
12. Wold, A.; Arnott, R.J.; Whipple, E.; Goodenough, J.B. Crystallographic Transitions in Several Chromium Spinel Systems. *J. Appl. Phys.* **1963**, *34*, 1085–1086. [[CrossRef](#)]
13. Ohtani, S.; Watanabe, Y.; Saito, M.; Abe, N.; Taniguchi, K.; Sagayama, H.; Arima, T.; Watanabe, M.; Noda, Y. Orbital dilution effect in ferrimagnetic  $\text{Fe}_{1-x}\text{Mn}_x\text{Cr}_2\text{O}_4$ : Competition between anharmonic lattice potential and spin-orbit coupling. *J. Phys. Condens. Matter* **2010**, *22*, 176003. [[CrossRef](#)]
14. Ma, J.; Garlea, V.O.; Rondinone, A.; Aczel, A.A.; Calder, S.; Dela Cruz, C.; Sinclair, R.; Tian, W.; Chi, S.; Kiswandhi, A.; et al. Magnetic and structural phase transitions in the spinel compound  $\text{Fe}_{1+x}\text{Cr}_{2-x}\text{O}_4$ . *Phys. Rev. B* **2014**, *89*, 134106. [[CrossRef](#)]
15. Hastings, J.M.; Corless, L.M. Magnetic Structure of Manganese Chromite. *Phys. Rev.* **1962**, *126*, 556–565. [[CrossRef](#)]
16. Menyuk, N.; Dwight, K.; Lyons, D.; Kaplan, T.A. Classical Theory of the Ground Spin-State in Normal Tetragonal Spinel. I. Néel, Yafet-Kittel, and Collinear Antiferromagnetic Modes. *Phys. Rev.* **1962**, *127*, 1983–1996. [[CrossRef](#)]
17. Nakamura, S.; Fuwa, A. Spin order in  $\text{FeCr}_2\text{O}_4$  observed by Mössbauer spectroscopy. *Phys. Procedia* **2015**, *75*, 747–754. [[CrossRef](#)]
18. Tomiyasu, K.; Kagomiya, I. Magnetic structure of  $\text{NiCr}_2\text{O}_4$  studied by neutron scattering and magnetization measurements. *J. Phys. Soc. Jpn.* **2004**, *73*, 2539–2542. [[CrossRef](#)]
19. Tanaka, M.; Tokoro, T.; Aiyama, Y. Jahn-Teller Effects on Mössbauer Spectra of  $\text{Fe}_{57}$  in  $\text{FeCr}_2\text{O}_4$  and  $\text{FeV}_2\text{O}_4$ . *J. Phys. Soc. Jpn.* **1966**, *21*, 262–267. [[CrossRef](#)]
20. Singh, K.; Maignan, A.; Simon, C.; Martin, C.  $\text{FeCr}_2\text{O}_4$  and  $\text{CoCr}_2\text{O}_4$  spinels: Multiferroicity in the collinear magnetic state? *Appl. Phys. Lett.* **2011**, *99*, 172903. [[CrossRef](#)]
21. Yusupov, R.V.; Cherosov, M.A.; Gabbasov, B.F.; Vasin, K.V.; Batulin, R.G.; Kiyamov, A.G.; Eremin, M.V. Magnetic Irreversibilities and Nonreciprocity of the Microwave Absorption of  $\text{FeCr}_2\text{O}_4$  Spinel. *JETP Lett.* **2022**, *115*, 190–196. [[CrossRef](#)]
22. Yu, S.; Gao, B.; Kim, J.W.; Cheong, S.-W.; Man, M.K.L.; Madéo, J.; Dani, K.M.; Talbayev, D. High-temperature terahertz optical diode effect without magnetic order in polar  $\text{FeZnMo}_3\text{O}_8$ . *Phys. Rev. Lett.* **2018**, *120*, 037601. [[CrossRef](#)] [[PubMed](#)]
23. Kézsmárki, I.; Szaller, D.; Bordács, S.; Kocsis, V.; Tokunaga, Y.; Taguchi, Y.; Murakawa, H.; Tokura, Y.; Engelkamp, H.; Rößm, T.; et al. One-way transparency of four-coloured spin-wave excitations in multiferroic materials. *Nat. Commun.* **2014**, *5*, 3203. [[CrossRef](#)] [[PubMed](#)]
24. Cherosov, M.A.; Zinnatullin, A.L.; Batulin, R.G.; Kiyamov, A.G.; Yusupov, R.V.; Taurskii, D.A. Mössbauer effect study of a polycrystalline  $\text{Fe}_{1+x}\text{Cr}_{2-x}\text{O}_4$  spinel grown by solid-state synthesis. *J. Phys. Conf. Ser.* **2022**, *2164*, 012067. [[CrossRef](#)]
25. Klemme, S.; O'Neill, H.S.C.; Schnelle, W.; Gmelin, E. The heat capacity of  $\text{MgCr}_2\text{O}_4$ ,  $\text{FeCr}_2\text{O}_4$ , and  $\text{Cr}_2\text{O}_3$  at low temperatures and derived thermodynamic properties. *Am. Mineral.* **2000**, *85*, 1686–1693. [[CrossRef](#)]
26. Matsnev, M.E.; Rusakov, V.S. SpectrRelax: An application for Mössbauer spectra modeling and fitting. *AIP Conf. Proc.* **2012**, *1489*, 178–185. [[CrossRef](#)]
27. Lenaz, D.; Skogby, H.; Princivalle, F.; Halenius, U. Structural changes and valence states in the  $\text{MgCr}_2\text{O}_4$ – $\text{FeCr}_2\text{O}_4$  solid solution series. *Phys. Chem. Miner.* **2004**, *31*, 633–642. [[CrossRef](#)]
28. Matsnev, M.E.; Rusakov, V.S. Study of spatial spin-modulated structures by Mössbauer spectroscopy using SpectrRelax. *AIP Conf. Proc.* **2014**, *1622*, 40–49. [[CrossRef](#)]
29. Kose, K.; Iida, S. Interacting phase transitions in  $\text{Fe}_{1+x}\text{Cr}_{2-x}\text{O}_4$  ( $0 \leq x \leq 0.4$ ). *J. Appl. Phys.* **1984**, *55*, 2321. [[CrossRef](#)]
30. Prodan, L.; Yasin, S.; Jesche, A.; Deisenhofer, J.; Krug von Nidda, H.-A.; Mayr, F.; Zherlitsyn, S.; Wosnitza, J.; Loidl, A.; Tsurkan, V. Unusual field-induced spin reorientation in  $\text{FeCr}_2\text{S}_4$ : Field tuning of the Jahn-Teller state. *Phys. Rev. B* **2021**, *104*, L020410. [[CrossRef](#)]
31. Wang, H.O.; Zhao, P.; Sun, J.J.; Tan, W.S.; Su, K.P.; Huang, S.; Huo, D.X. Investigation of magnetic response of charge ordering in half-doped  $\text{La}_{0.5}\text{Ca}_{0.5}\text{MnO}_3$  manganite. *J. Mater. Sci. Mater. Electron.* **2018**, *29*, 13176–13179. [[CrossRef](#)]